JOURNAL OF GEOPHYSICAL RESEARCH, VOL. 113, D00C05, doi:10.1029/2007JD009457, 2008

Aerosol optical depths over North Africa: 2. Modeling and model validation

Glenn Greed,[1] Jim M. Haywood,[1] Sean Milton,[1] Andreas Keil,[1] Sundar Christopher,[2] Pawan Gupta,[2] and Eleanor J. Highwood[3]

Received 4 October 2007; revised 7 March 2008; accepted 17 March 2008; published 29 July 2008.

[1] An operational dust forecasting model is developed by including the Met Office Hadley Centre climate model dust parameterization scheme, within a Met Office regional numerical weather prediction (NWP) model. The model includes parameterizations for dust uplift, dust transport, and dust deposition in six discrete size bins and provides diagnostics such as the aerosol optical depth. The results are compared against surface and satellite remote sensing measurements and against in situ measurements from the Facility for Atmospheric Airborne Measurements for a case study when a strong dust event was forecast. Comparisons are also performed against satellite and surface instrumentation for the entire month of August. The case study shows that this Saharan dust NWP model can provide very good guidance of dust events, as much as 42 h ahead. The analysis of monthly data suggests that the mean and variability in the dust model is also well represented.

Citation: Greed, G., J. M. Haywood, S. Milton, A. Keil, S. Christopher, P. Gupta, and E. J. Highwood (2008), Aerosol optical depths over North Africa: 2. Modeling and model validation, *J. Geophys. Res.*, *113*, D00C05, doi:10.1029/2007JD009457.

1. Introduction

[2] Aerosols have received considerable attention over the last two decades [e.g., *Haywood and Boucher*, 2000; *Intergovernmental Panel on Climate Change*, 2001]. They scatter and absorb solar and terrestrial radiation (the direct effect) and alter the physical, optical, and lifetime properties of cloud (the indirect effect). Mineral dust aerosol is an important atmospheric component for a number of reasons. Because the size distribution of mineral dust contains both fine (submicron) and coarse (supermicron) particles it exerts a significant influence on both solar [e.g., *Haywood et al.*, 2003] and terrestrial radiation [*Highwood et al.*, 2003; *Haywood et al.*, 2005] and therefore effects the energy balance of the Earth/atmosphere system. A number of dust/aerosol short-range prediction systems have been developed in the last decade by various universities and research institutes, some of which are now run routinely in operational frameworks. *Uno et al.* [2006] provides details of eight different dust models run over Asia in the Dust Model Intercomparison Project (DMIP), some of which are run routinely. These models include the Coupled Ocean Atmospheric Mesoscale Prediction System (COAMPS) [*Liu et al.*, 2003], the Asian Dust aerosol Model (ADAM) [*In and Park*, 2003] run by the Korean Meteorological Agency, and the Model of Aerosol Species in the Global Atmosphere (MASINGAR) [*Tanaka and Chiba*, 2005] run for the Asian region by the Japanese Meteorological Agency.

[3] Dust models that are run routinely for the north African and Mediterranean domains include the U.S. Navy Aerosol Analysis and Prediction System (NAAPS) [*Christensen*, 1997], the Dust Regional Atmospheric Model (DREAM) [*Nickovic et al.*, 2001] run by the Barcelona Supercomputing Centre and Tel Aviv University (http://www.bsc.es), the SKIRON model of the University of Athens (http://forecast.uoa.gr/dustindx.html) [*Kallos et al.*, 1997] and the CHIMERE model of Laboratoire de Météorolgie Dynamique (http://euler.lmd.polytechnique.fr/GEMSchimere/) [*Menut et al.*, 2007]. These models have been operational for some time (e.g., the SKIRON model has been operational since 1998) and undergone considerable development and refinement of physical parameterizations [e.g., *Kishcha et al.*, 2007]. For example, single-bin schemes have been superceded by multiple bin schemes and the aerosol radiative properties have been fully coupled to radiative transfer codes [e.g., *Nickovic et al.*, 2001; *Pérez et al.*, 2006]. These operational models provide predictions of mineral dust outbreaks that are of use to both civilian and military customers.

[4] In this study we use the dust production, transport, and deposition scheme developed for the Met Office Hadley Centre climate model (*Woodward* [2001] hereafter W2001) within a relocatable version of the Met Office regional model (Crisis Area Mesoscale Model (CAMM) [*Greed*, 2005] to model outbreaks of mineral dust over North Africa. Because the dust scheme was originally developed for a relatively low spatial and temporal resolution climate model, the dust parameterization's uplift scheme required

[1]Met Office, Exeter, UK.
[2]Department of Atmospheric Sciences, University of Alabama in Huntsville, Huntsville, Alabama, USA.
[3]Department of Meteorology, Reading University, Reading, UK.

0148-0227/08/2007JD009457$09.00

retuning to provide suitable dust loads within the higher resolution (spatially and temporally) numerical weather prediction (NWP) models. Data from a major dust storm in March 2006 measured by the Atmospheric Radiation Measurements (ARM) mobile facility stationed in Niamey is used for retuning purposes [*Slingo et al.*, 2006; *Milton et al.*, 2008]. Once retuned, the CAMM is run for the entire month of August 2006. An independent validation strategy was developed including comparison of CAMM AODs with those retrieved from the Multiangle Imaging Spectro Radiometer (MISR), the Ozone Monitoring Instrument (OMI), Aerosol Robotic Network (AERONET) surface sites, and aircraft in situ measurements.

[5] Section 2 briefly describes the CAMM, the climate model dust scheme and the revisions made to the scheme during its implementation within the CAMM. Section 3 describes the multimeasurement validation strategy for assessing the performance of the model. Section 4 makes a comparison of the model fields against satellite, aircraft, and surface based measurements during a specific dust event over the period 21–24 August 2006. Section 5 extends the analysis period to make comparisons against data from the whole of August 2006. A discussion and conclusion are presented in section 6.

2. Description of the CAMM and the Dust Scheme

2.1. Met Office Unified Model

[6] The Met Office Unified Model (UM) [*Cullen*, 1993] is a flexible modeling tool used for global climate prediction (atmosphere only and/or coupled to an ocean), global NWP, regional NWP and high-resolution mesoscale models. The dynamical core is a nonhydrostatic two time level semi-implicit, semi-Lagrangian scheme described by *Davies et al.* [2005]. All UM configurations may use the same set of physics options, for example the two stream radiation scheme [*Edwards and Slingo*, 1996], the non local boundary layer scheme [*Lock et al.*, 2000; *Martin et al.*, 2000] and the Met Office Surface exchange scheme MOSES II [*Essery et al.*, 2003]. NWP configurations include data assimilation of satellite, radiosonde and surface observations and basic meteorological data from commercial aircraft. Met Office operational global and regional configurations use four-dimensional data assimilation system (4D-Var) [*Rawlins et al.*, 2007] while the CAMMs use a three dimensional data assimilation system (3D-var) [*Lorenc et al.*, 2000].

[7] The Met Office CAMMs are run operationally in support of allied military operations, disaster relief and research. Each CAMM is a relocated version of the Met Office North Atlantic-European (NAE) model [*Bush et al.*, 2006], and the CAMMs routinely follow Global and NAE model developments. No location specific tunings are normally made to the CAMMs.

2.2. Saharan CAMM and the Dust Scheme

[8] The Saharan CAMM domain is depicted in Figure 1 and has a resolution of $0.18^\circ \times 0.18^\circ$ ($\sim$20km), 38 levels in the vertical, a lid at $\sim$39km, with 13 levels representing the boundary layer. This CAMM differs from previous CAMMs with the inclusion of the Met Office Hadley Centre climate model dust parameterization scheme. The dust scheme is called every model time step. Dust emissions are dependent upon clay, silt and sand fractions, the vegetative fraction, soil moisture, a threshold friction velocity and the surface layer friction velocity. Dust transport is by the UM tracer advection scheme and the dust scheme also accounts for dry deposition from gravitational settling and turbulent mixing and wet deposition via precipitation scavenging. The radiative impact of the dust feeds back upon the NWP model fields. Radiative properties of dust are represented in each size bin by assuming spherical particles, appropriate refractive indices and by using Mie scattering theory to obtain the specific extinction coefficient, the asymmetry parameter and the single scattering albedo. These optical properties are averaged over six spectral bands in the solar part of the spectrum for use within the CAMM radiation code [*Edwards and Slingo*, 1996] and the dust fully interacts with both solar and terrestrial radiation which may be important in model evolution [e.g., *Pérez et al.*, 2006]. Optical depth diagnostics (AODs) at several wavelengths have been developed for each bin size and for the sum of the six bins. Except when explicitly stated, this study adopts AOD as representing the aerosol optical depth at a wavelength of 550 nm.

[9] As mentioned above, dust production is dependent upon fractions of clay, silt and sand detailed by the model soils data set and the soil moisture. The soil data set used in the climate model is of $1^\circ \times 1^\circ$ resolution [*Wilson and Henderson-Sellers*, 1985]. This is unsuitable for a NWP model as the data set is too coarse. For NWP configurations we use a soils data set from the International Geosphere Biosphere Programme (IGBP) [*Loveland and Belward*, 1998] of 1km resolution. The averaged fractions are interpolated onto the 20km model grid. Figure 1 compares the clay and sand fractions in North Africa region, when interpolated onto the Saharan model 20km grid, note the significant extra resolved detail in the IGBP data set. The Met Office operational global model soil moisture [*Best and Maisey*, 2002] is interpolated onto the CAMM grid, providing a soil moisture field that may respond to recent local precipitation events.

[10] Since the initial study of W2001, further developments of the dust scheme within the global climate model have been implemented to provide reasonable dust loadings. These revisions include

[11] 1. Horizontal dust flux calculations include sand particles up to 2000 μm diameter. The vertical flux is still assumed to consist only of particles between 0.06 and 60 μm.

[12] 2. The size distribution of vertical flux is assumed to follow parent soil size distribution rather than that of the horizontal flux.

[13] 3. Excessive dust emissions on steep orographic slopes is inhibited.

[14] Here we provide a brief overview of the updated dust uplift formulation as used in the NWP configurations. The dust scheme is an upgraded version of W2001 developed for the climate configuration of the UM, for a detailed description of the original scheme we refer the reader to W2001.

[15] Transported dust is specified in six size divisions spanning 0.06–60 μm in diameter. The dust uplift scheme is

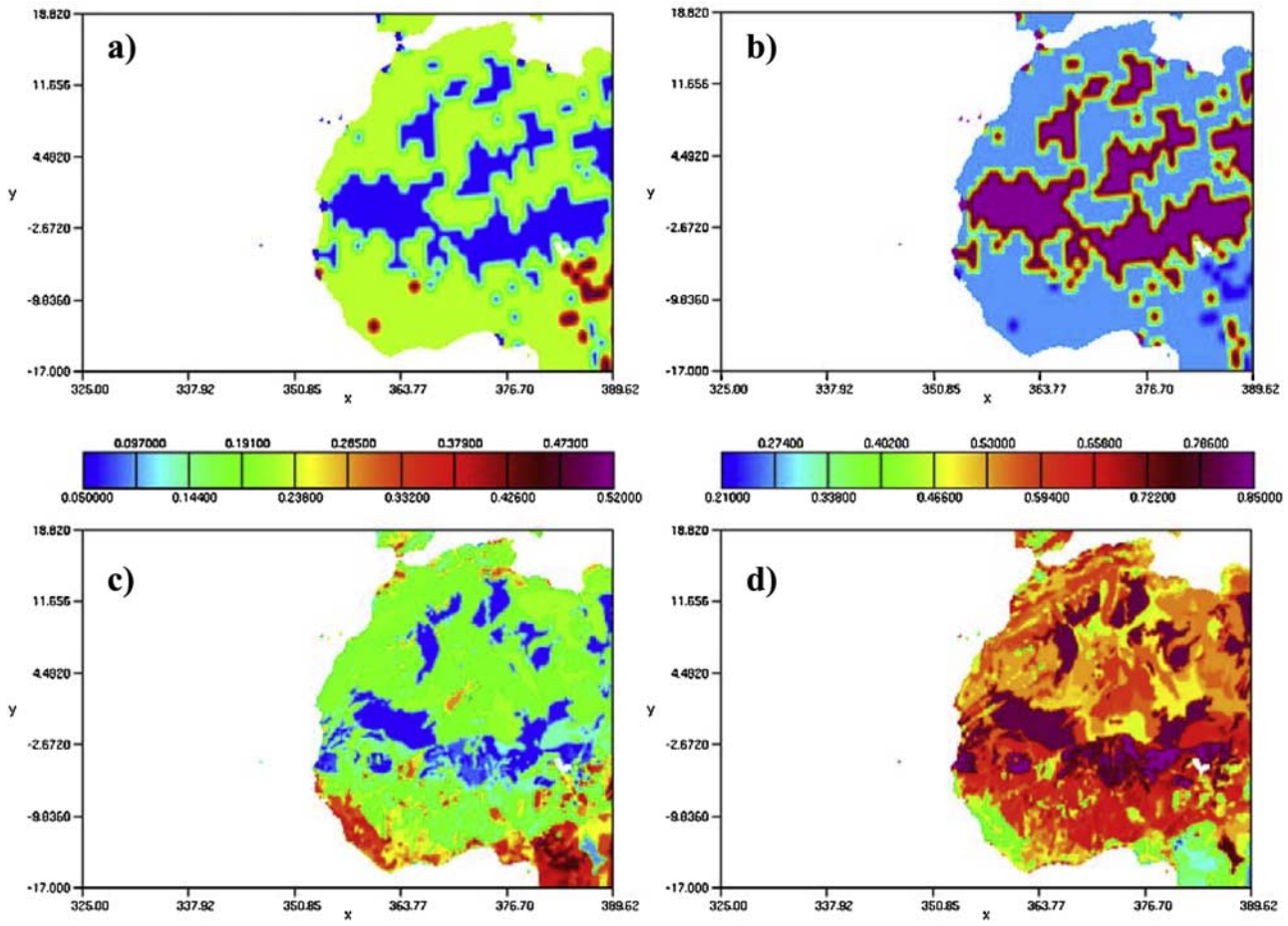

Figure 1. The soil fraction of (a) clay, (b) sand from *Wilson and Henderson-Sellers* [1985]; (c) clay, and (d) sand from IGBP.

a modified form of *Marticorena and Bergametti* [1997]. The dust flux (G) is defined as

$$G = 0.01H.10^{(13.4F_c - 6)}\left(\frac{M_{\text{rel}}}{M_{\text{rel}}^{\text{tot}}}\right), \quad (1)$$

where F_c is the clay fraction, M_{rel} is the ratio of mass of dust in a size division to total mass and $M_{\text{rel}}^{\text{tot}}$ is a similar ratio but for the sum of the six dust bins mass to total mass. Horizontal flux (H) is defined by

$$H = 2.61\rho(1-\nu)2U^{*3}\left(1+\frac{U_t^*}{U^*}\right)\left(1-\left(\frac{U_t^*}{U^*}\right)^2\right)\frac{M_{\text{rel}}}{g}, \quad (2)$$

where ν is the vegetation fraction, ρ is the air density, g is the acceleration due to gravity, U^* is the surface layer friction velocity, and U_t^* is the threshold friction velocity

$$U_t^* = A\log_{10}\left(D_{\text{rep}}\right) + BW + C, \quad (3)$$

where A, B, and C are empirical constants; D_{rep} is a bin particle diameter, and W is the 10 cm deep soil moisture. The use of a linear dependence on soil moisture is taken from *Hotta et al.* [1984].

[16] In addition to the developments in the global dust scheme since W2001, the dust parameterization uplift scheme required a minor retuning to provide suitable forecasts in the NWP models. A major Saharan dust event during early March 1996 [*Slingo et al.*, 2006] provided suitable observations to tune the dust uplift scheme. *Milton et al.* [2008] compare global model forecasts with measurements from the ARM mobile facility which was located in Niamey, Niger, for 2006. *Milton et al.* [2008] found that the climate empirical constants (equation (3)) in the Saharan CAMM provided good spatial guidance of the dust event albeit with too little dust. In sensitivity tests with the Saharan CAMM and a global model (N216, 90km resolution at the equator) *Milton et al.* [2008] found a value of C of -0.15 ms^{-1} yielded a reasonable range of AODs for the event while C is 0 ms^{-1} in the climate model; a C of -0.15 ms^{-1} is adopted in the CAMM.

[17] Following the retuning, the Saharan CAMM was run in operational mode twice daily out to $T + 48$, from 0600 UTC and 1800 UTC throughout August 2006. The boundary conditions were supplied by the Met Office operational global model (N320 L50, 60km resolution at the equator.).

[18] The Saharan CAMM is initiated in mid-July 2006 with zero dust. The dust scheme is completely free running in terms of emissions, transport and deposition; it does not assimilate dust within the data assimilation cycle and there

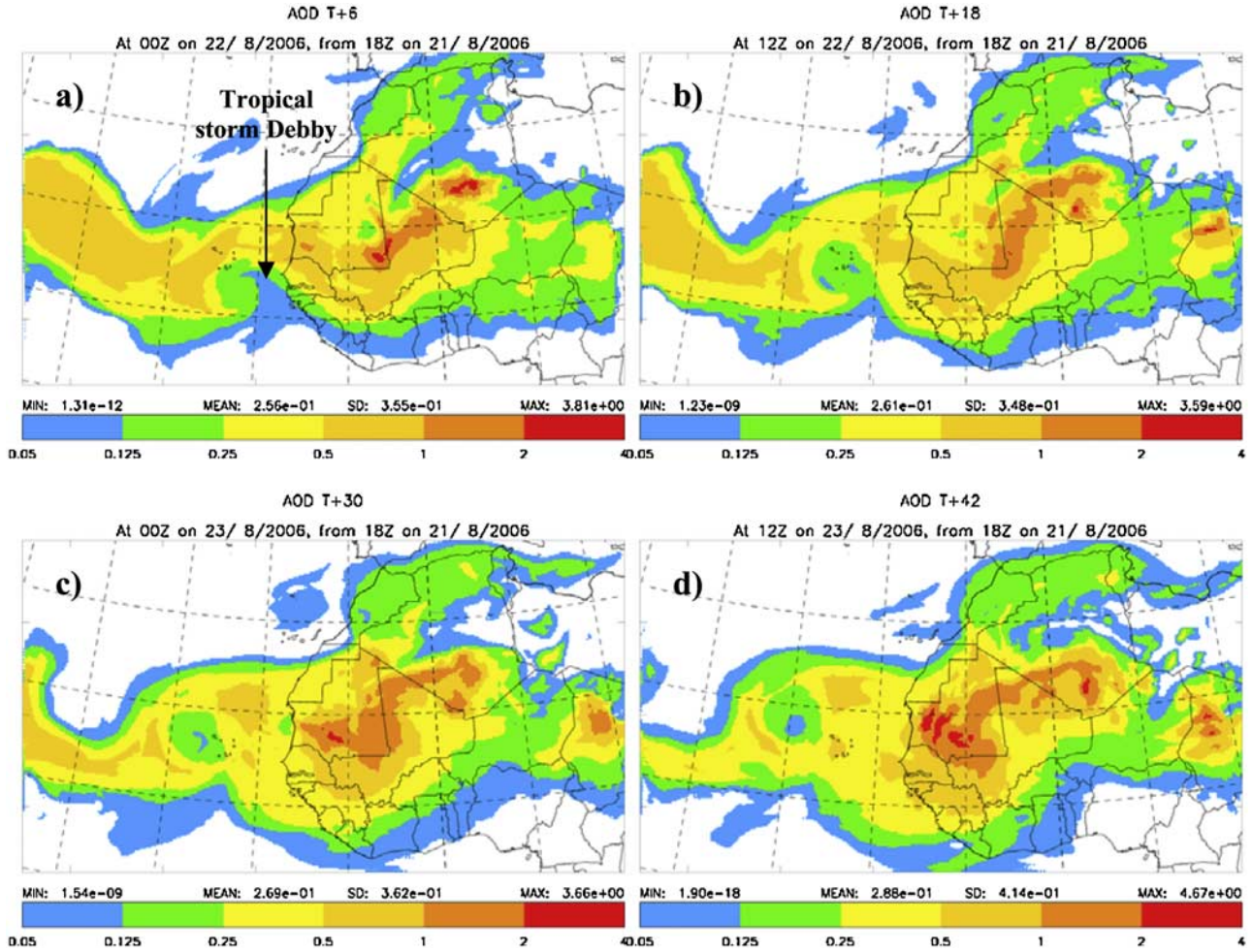

Figure 2. Forecasts of the aerosol optical depth at 550 nm for the dust storm in Mauritania from the CAMM for the 23 August 2006 for (a) $T + 6$, (b) $T + 18$, (c) $T + 30$, and (d) $T + 42$ h. The advection of the dust storm from east to west across North Africa is clearly shown.

is no intervention mechanism to initiate observed dust events. Dust is only sourced from the soils data set and consequently resuspension of transported dust is not explicitly accounted for in the model, but only implicitly in the soil data set which could result in the source areas being significantly underestimated. Additionally, there is no dust transport into the model domain through the model boundaries. Both of these model weaknesses will obviously impact upon dust predictability and background dust levels. Furthermore, intense, smaller-scale dust storms initiated by intense convective events, are also unlikely to be fully resolved within a 20km model, although the combined dust uplift from these convective events may be significant during the rainy season of the African monsoon [e.g., *Sterk*, 2003].

3. Validation Strategy

[19] The results from the CAMM dust scheme may be compared against a variety of observations at a variety of different temporal scales. We choose two periods for investigation; the first being a case study co-incident with BAe 146 aircraft observations, and the second being a comparison performed over the entire month. In the latter we consider short-range CAMM dust forecasts to minimize NWP errors.

[20] The Facility for Atmospheric Airborne Measurement (FAAM) BAe 146 aircraft encountered a dust event in Mauritania on the 23 August 2006. The BAe 146 aircraft is Europe's most comprehensively equipped meteorological research aircraft, and was based in Dakar while participating in the Dust Outflow and Deposition to the Ocean (DODO2) measurement campaign. Six dedicated flights were performed over the period 22–28 August 2006. While many of the flights were over the ocean regions, the flight on the 23 August specifically targeted the high-intensity dust storm over Mauritania forecast by the CAMM. Because only a single large dust event (AOD > 1) was encountered by the BAe 146 aircraft during the DODO2 period, aircraft observations of intense dust events are not available at other times. Aircraft measurements include the aerosol size distribution, the aerosol scattering and the aerosol absorption which are available for validation of the model [e.g., *Highwood et al.*, 2007]. Validation measurements from the BAe 146 instruments include information on the vertical profile of mineral dust which cannot be inferred

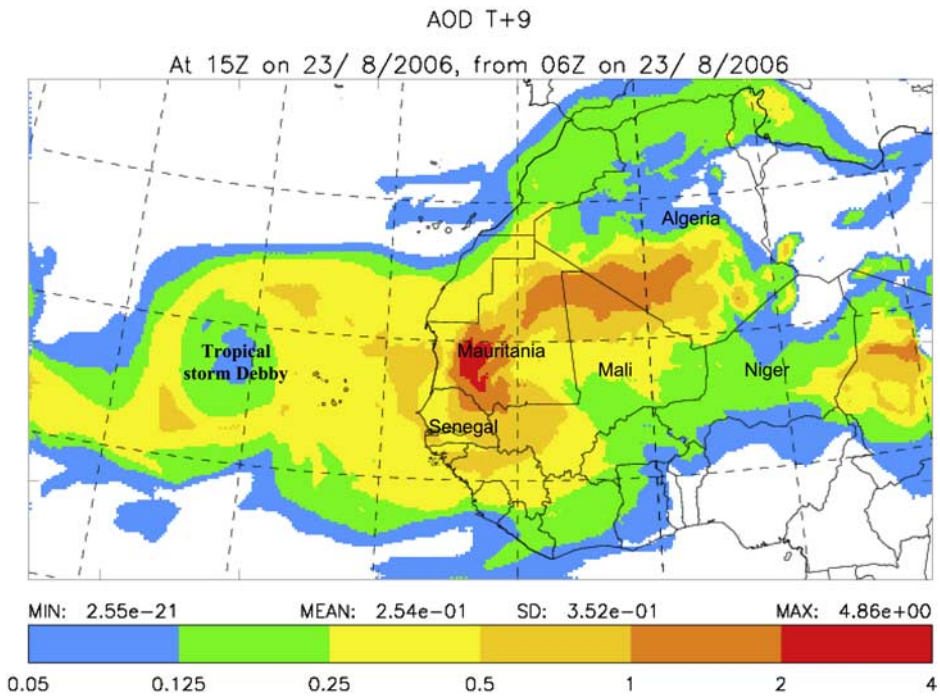

Figure 3. A short-range $T + 9$ forecast showing the dust storm over Mauritania, northern Mali, and southern Algeria. The location of tropical storm Debby is clearly identified by the reduced AODs over the ocean caused by wet deposition.

from the satellite or Sun photometer remote sensing techniques.

[21] Derivation of reliable AODs from satellite retrievals over desert surfaces continues to be problematic because the high surface reflectance means that the fractional contribution to satellite detected radiances from an overlying aerosol layer is low at visible wavelengths. The spatial variability in the surface reflectance and uncertainties in modeling the bidirectional reflectance function provide additional complexities. MISR uses its multiangle viewing capability to reduce these problems and provides reasonably well-validated AOD data over desert surfaces [e.g., *Martonchik et al.*, 2004; *Christopher et al.*, 2008]. However, the limited swath width means that the spatial coverage is inadequate for making comparisons of the dust event on the 23 August. The surface reflectance of desert drops significantly in the UV, which means that broad swath width instruments such as the Total Ozone Mapping Spectrometer (TOMS) instrument, which was a forerunner to the OMI instrument can be used to derive a semiquantitative Aerosol Index. However, the Aerosol Index is dependent upon the altitude of the aerosol, the single scattering albedo, and the aerosol optical depth (AOD) [e.g., *Hsu et al.*, 1999]. Other studies have developed methods for converting the Aerosol Index from TOMS to more quantitative AODs [e.g., *Ginoux and Torres*, 2003]. Here we extend the approach of *Haywood et al.* [2005] and use multiyear correlation and regression of TOMS/OMI AIs to MISR AODs to provide quantitative AOD data for assessing model performance [*Christopher et al.*, 2008]. Satellite data from both the case study of 23 August and the monthly mean for August are used to investigate the model performance.

[22] The AERONET Sun photometer network provides high-quality AOD data at selected sites across the Earth [*Holben et al.*, 1998]. While many areas close to habitation have a relatively high spatial coverage, areas close to the Saharan dust plume are data sparse. Only the site of Dakar in Senegal is in reasonable proximity to the dust event and currently provides suitably quality controlled (Level 2) data for both the case study and the month long period.

4. Case Study of 23 August 2006

[23] CAMM forecasts charts of forecast AOD, available twice daily from 0600 to1800 UT model runs, proved extremely useful for the BAe 146 mission flight planning team. Figures 2a–2d presents the forecast evolution of dust AODs over a period of 36 h, from $T + 6$ to $T + 42$ from the 1800 UT 21 August 2006 model run. Significant dust is lifted from Algeria and Mali and then propagates westward toward Mauritania. This forecast provided a useful heads up of the upcoming dust event. Figure 3 depicts the short-range $T + 9$ forecast, valid 1500 UT 23 August 2006, of AOD at a wavelength of 550 nm. The dust event is clearly discernible over Mauritania with the modeled aerosol AOD exceeding 2. The flight crew engaged significant dust in the area between1430 and 1630 UT, as we shall see. To validate the model, three different validation tools are used; satellite retrievals, AERONET observations, and aircraft observations.

[24] Satellite retrievals that observe the dust storm are limited owing to the (relatively) small spatial scale of the dust storm and the (relatively) small swath width of aerosol retrievals from dedicated satellite instruments that are able to make measurements over bright surfaces. For this reason, *Christopher et al.* [2008] make use of correlation relationships between the narrow swath MISR instrument on board

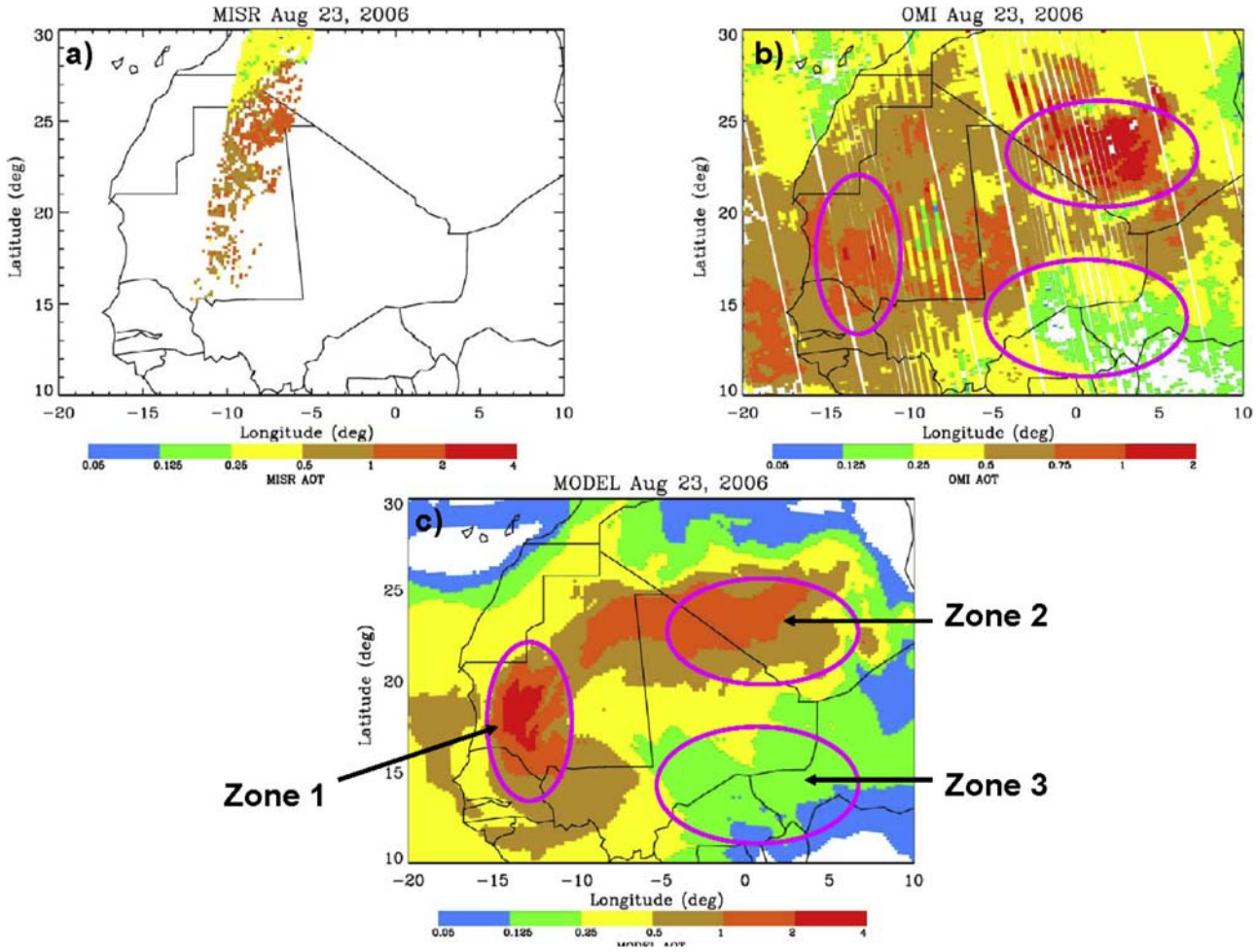

Figure 4. AODs at 550 nm from (a) MISR, (b) OMI, and (c) CAMM. The limited swath width of MISR is clearly evident. Note that Figures 4a and 4c have a different scale than Figure 4b.

the TERRA satellite and the broad swath width OMI instrument on board the AURA satellite.

[25] A comparison of the model and the satellite derived products are shown in Figure 4 over a more limited model domain. The MISR data in Figure 4a shows AODs in excess of 1 in North Eastern Mauritania close to the border with Algeria. The limited swath width makes quantitative assessment of the model performance difficult, although there is some evidence that the widespread AODs of between 0.5 and 1.0 over much of Mauritania are also evident in the model (Figure 4c). Figure 4b shows the AOD derived from the OMI instrument. The comparison of the OMI AOD with that in some regions of heavy model loading (e.g., Zone 1) shows the model AODs are higher than those derived from OMI (note that Figures 4b and 4c are plotted on different scales) while in other regions (e.g., Zone 2) there appears to be a reasonable correspondence between the magnitude of the modeled and OMI AODs. The intrusion of less turbid air shown in Zone 3 are evident in both the model and the OMI AODs. While there are some differences in the spatial distribution of the AODs from the model with those from the two satellite instruments, the spatial coherence of the forecast and observed dust plumes and low turbidity regions is encouraging, and gives confidence that the model is able to forecast the spatial scale and geographic location of significant dust events.

[26] The AOD at 550 nm from the single-grid box that encompasses the M'Bour site situated close to Dakar, Senegal is compared against that from the AERONET site for the intensive period 21–24 August 2006 in Figure 5. The AERONET data shows that the variability of the dust AOD within a day can be significant, with the AOD on the 21 August ranging from approximately 0.1 to 0.6. Over the limited time period investigated here, the CAMM model generally shows less variability, except for the 24 August, which is when the dust event identified over Mauritania on the 23 August is forecast to influence Dakar. Encouragingly, the CAMM model and the AERONET AODs are in statistical agreement with each other on all four of the days considered during this period. The mean and the standard deviation of the AOD are summarized in Table 1. The mean AODs from AERONET and from the CAMM are not significantly different at the 2 standard deviation level, and only the data of the 21 August shows a significant difference at the 1 standard deviation level. The low AODs evident in the AERONET data on the 21 August are due to the passage of tropical storm Debby to the South of Dakar which caused aerosol wash out via wet deposition. This caused not only steep temporal gradients in the AOD in the

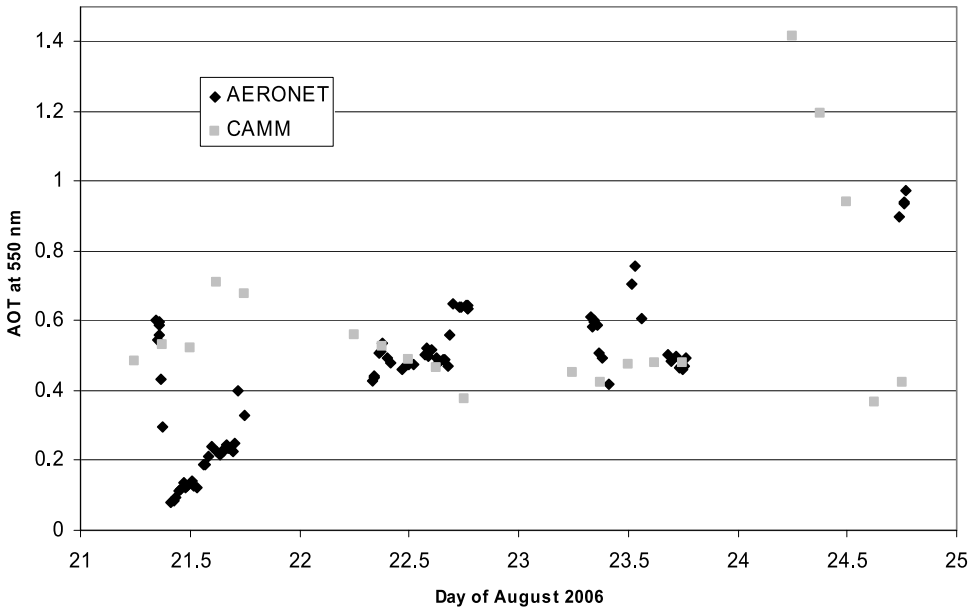

Figure 5. The AOD at 550 nm from the CAMM and AERONET site at M'Bour near Dakar, Senegal for the period 21–24 August 2006. Only CAMM data from 0600–1800 UT are shown as this roughly corresponds to times when AERONET data can be retrieved (sunlight hours only).

Dakar area on the 21 August as evidenced by the large variability in the AERONET data (Figure 5), but also steep geographic gradients in the AOD as evidenced by Figure 2a, which clearly shows AODs of less than 0.125 to the south of Dakar and AODs of greater than 0.5 to the north of Dakar. The reasons for the differences between the AODs on the 21 August are most likely related to the close proximity of tropical storm Debby; positional errors will significantly impact dust uplift and deposition via rainout. The model resolution (20km) is unlikely to resolve the true wind gradients and the associated rainfall totals. The interpolated soil moisture field may also be deficient in the wake of Debby, allowing the CAMM to lift erroneous dust without the inhibiting soil moisture.

[27] Other reasons for the differences in AODs may be the result of other aforementioned known model weaknesses; the dust availability data set, the lack of accounting for the transport of dust through boundaries and the models inability to resolve small-scale convective events.

[28] The BAe 146 took off from Dakar at 1250 UT and performed a sortie of approximately 4.75 h. The track of the BAe 146 aircraft is shown in Figure 6. The aircraft encountered heavy dust loadings during the period 1430–1630 UT while operating in the region 18–19°N, 13–15°W, an area that corresponds to the high AODs derived from the OMI satellite instrument, and derived by the CAMM. Two deep vertical profiles were made with the aircraft ascending/descending at 500–1000ft/min within the dust layer. Aerosol scattering was determined at 3 wavelengths (450, 550, and 700 nm) with a TSI 3563 nephelometer and aerosol absorption with a Radiance Research Particle Soot Absorption Photometer (PSAP) via a Rosemount inlet. As shown by *Haywood et al.* [2003] corrections were made for missing scattering owing to the internal geometry of the nephelometer [*Anderson and Ogren*, 1998], and for the reduced inlet efficiency for supermicron particles, while the corrections from *Bond et al.* [1999] were applied to the PSAP. The results from the two vertical profiles are shown in Figure 7. The scattering shows little variation across the three wavelengths of the nephelometer, indicating that the aerosols are dominated by the large dust particles [e.g., *Haywood et al.*, 2003]. There is a significant difference between the two profiles in that the first profile shown in Figure 7a shows much reduced scattering when compared to Figure 7b which shows a deeper, thicker mineral dust plume. The AODs at wavelength λ may be calculated from the equation

$$\mathrm{AOD}_\lambda = \int_z k_{\mathrm{ext}\lambda}\mathrm{mmr}dz, \tag{4}$$

where the specific extinction coefficient, k_{ext}, is in $\mathrm{m^2g^{-1}}$, mmr is the mass mixing ratio in $\mathrm{gm^{-3}}$, and z is the altitude in meters. The nephelometer essentially measures the aerosol scattering, $Q_{\mathrm{sca}\lambda}$, in units of $\mathrm{m^{-1}}$ which is the product of the specific scattering coefficient, k_{sca} and mmr, and the PSAP measures the aerosol absorption, $Q_{\mathrm{abs}\lambda}$ in units of $\mathrm{m^{-1}}$ which is the product of the specific absorption

Table 1. Showing the Mean and the Standard Deviation in the AOD at 550 nm From the AERONET Site at M'Bour Near Dakar, Senegal, and the Corresponding AOD Predicted by the CAMM Model

	AOD AERONET		AOD CAMM	
Day	Mean	Standard Deviation	Mean	Standard Deviation
21 Aug	0.26	0.16	0.58	0.10
22 Aug	0.52	0.07	0.48	0.07
23 Aug	0.54	0.09	0.46	0.02
24 Aug	0.94	0.03	0.87	0.46

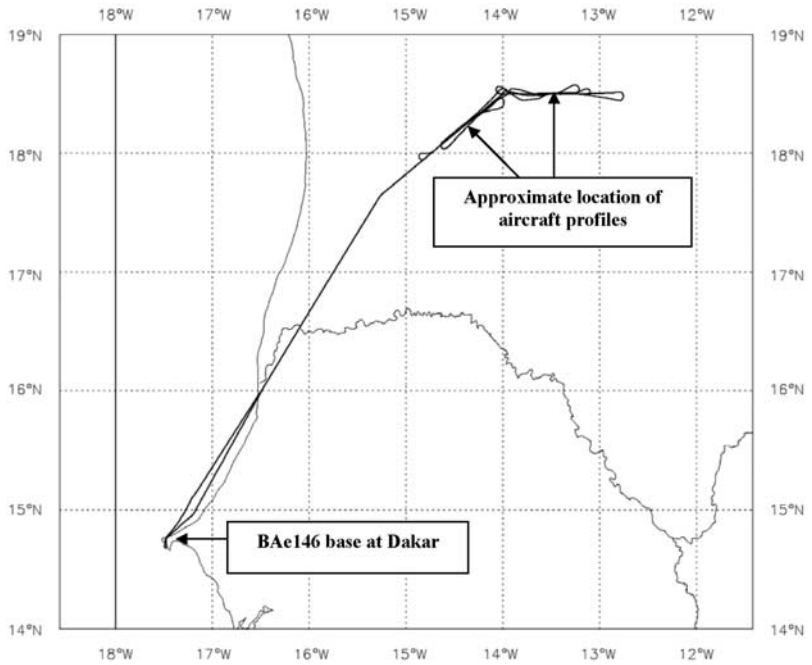

Figure 6. The track of the BAe 146 aircraft on the 23 August 2006. The majority of the scientific flying was performed between 15 and 13°W and 18 and19°N.

coefficient k_{abs} and mmr. The single scattering albedo, ω_o, is defined by

$$\omega_{o\lambda} = \frac{Q_{\text{sca}\lambda}}{Q_{\text{sca}\lambda} + Q_{\text{abs}\lambda}} \tag{5}$$

and hence

$$\text{AOD}_\lambda = \int_s \frac{k_{\text{sca}\lambda}}{\omega_{0\lambda}} \text{mmr} dz. \tag{6}$$

[29] The single scattering albedo determined from within the dust layer from the two profiles shown in Figures 7a and 7b are 0.93 and 0.97 (standard deviation 0.03). The total AOD derived at 550 nm is estimated to be 0.48 from Figure 7a and 1.06 from Figure 7b with an uncertainty of around 30% owing mainly to the uncertainties in correcting for the deficiencies in the aerosol inlet which fails to capture the largest particles [*Haywood et al.*, 2003]. The distance between the mean position of the vertical profiles was approximately 110 km indicating significant spatial variability in the AOD.

[30] A comparison of the vertical profiles derived from the aircraft instrumentation against that from the model is shown in Figures 7c and 7d. Figures 7c and 7d show that there are essentially two layers of dust represented in the model; a surface layer extending from the surface to 2000–3000 m, and an elevated layer extending from 2000–3000 m to 7000–8000 m. The wavelength dependence of the scattering differs when compared to the observed scattering, with the model showing blue scattering which is greater than green scattering which is greater than red scattering (cf. Figure 7a and 7b). This is because the modeled dust size distribution is biased to small sizes when compared to the in situ measurements. In addition, the model appears to underpredict the peak surface layer aerosol scattering in Figure 7c. However, there are a number of other metrics by which the model can be considered a success. First the modeled AOD derived from the two profiles shown is 0.40 and 1.04 which is in agreement with the measurements given the range in measurement uncertainties. Second, the model captures the spatial variation in the AOD reasonably over the 100 km spatial scales that are measured by the aircraft. Third the capping of the surface layer compares favorably with the observations. Fourthly, the general evolution of the surface layer from being capped at ~2000 m (Figure 7c) to being capped at ~3000 m (Figure 7d) as the dust layer thickens is also captured by the model.

5. Comparison of the Monthly Mean Data From August 2006

[31] As previously noted, the validation strategy for the modeled monthly mean fields includes comparison against available satellite data and comparison against AERONET data from Dakar.

[32] Satellite data used in the validation of the model include the MISR monthly mean AOD, and that from OMI derived using the method of *Christopher et al.* [2008] (Figure 8). MISR AODs shown in Figure 8a now reveal a reasonable coverage in the monthly mean because these areas are free from significant cloud cover during this time period. The exception is to the south of the region where cloud associated with the ITCZ means that averaging over a month still does not provide full coverage. Comparison of the AOD retrieved from MISR and OMI reveals a close similarity between the magnitude and spatial distributions of the AODs. The agreement between the AODs is to be expected because multiyear MISR data is regressed against

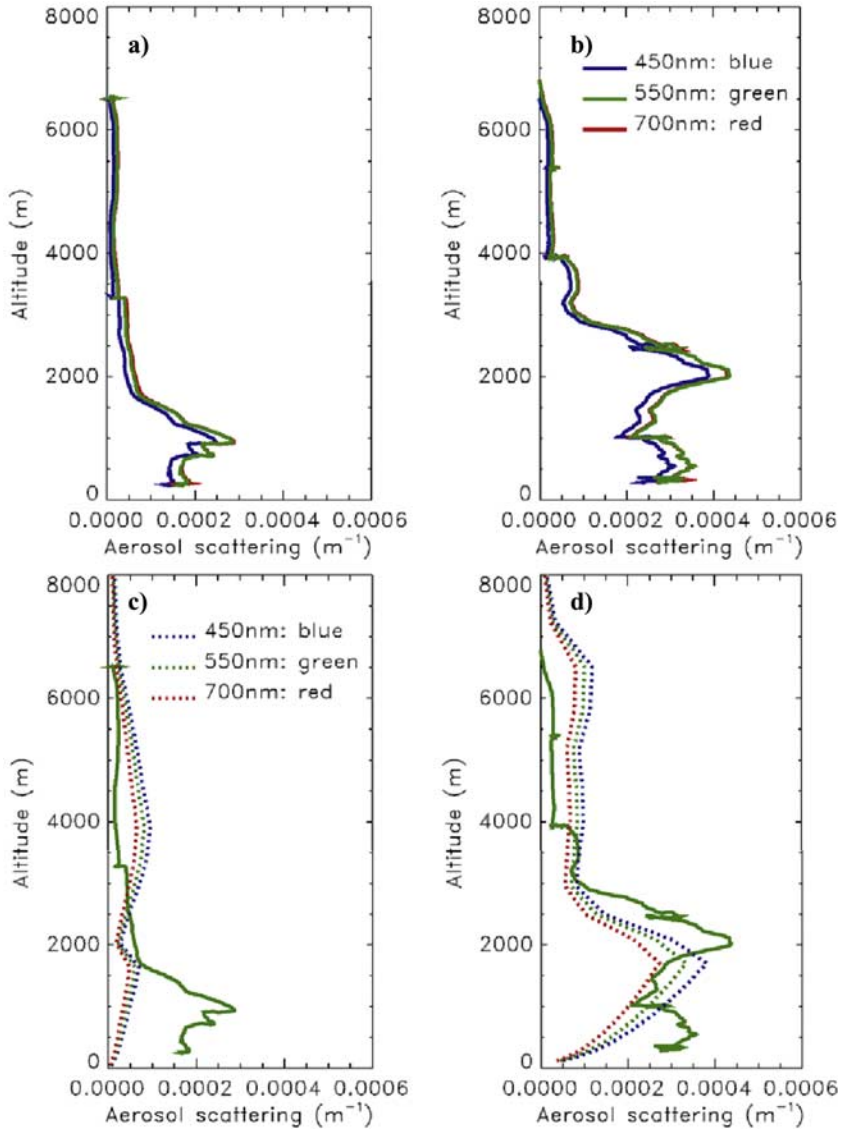

Figure 7. (a and b) The aerosol scattering at 450, 550, and 700 nm derived from the nephelometer measurements onboard the BAe 146 aircraft during two deep vertical profiles. The mean location for Figure 7a was approximately 18.2°N, 14.5°W, while that for Figure 7b was 18.5°N, 13.5°W. (c and d) The aerosol scattering at 450, 550, and 700 nm derived from the model (dotted lines), together with the aerosol scattering at 550 nm from the nephelometer measurements (solid green lines).

OMI Aerosol Index to provide an OMI AOD [*Christopher et al.*, 2008]. There are some differences however in the spatial distribution of the AODs between MISR and OMI particularly over the Western Sahara, southern Algeria, and over Niger. These differences occur because of different spatial sampling frequencies between the two instruments. OMI provides near full coverage each day while the repeat interval for MISR is approximately once every 6–7 days in this region. Thus monthly mean MISR data is frequently made up from AODS from four to five individual overpasses which can result in dust storms being either over or under sampled in the monthly mean. Multiyear analyses would reduce any potential biases. Comparison of the model with MISR and OMI AODs reveal a generally reasonable spatial distribution and magnitude. The model is not perfect however; regions such as Niger reveal that the AOD is rather underestimated in the model when compared to both MISR and OMI. Note that at extreme northern and southern latitudes within Figure 7c, the model is not expected to give agreement with the observations because it does not contain any other aerosol species such as sea salt or biogenic aerosol which can contribute significantly to the total AOD.

[33] Scatterplots of the MISR AOD and OMI AOD against the CAMM AOD are shown in Figures 9a and 9b, respectively. The MISR and OMI AODS are correlated with the model AOD (R = 0.67 and R = 0.75), and the relationships derived from a linear regression are

$$\mathrm{AOD_{CAMM}} = 0.68\mathrm{AOD_{MISR}} + 0.10$$

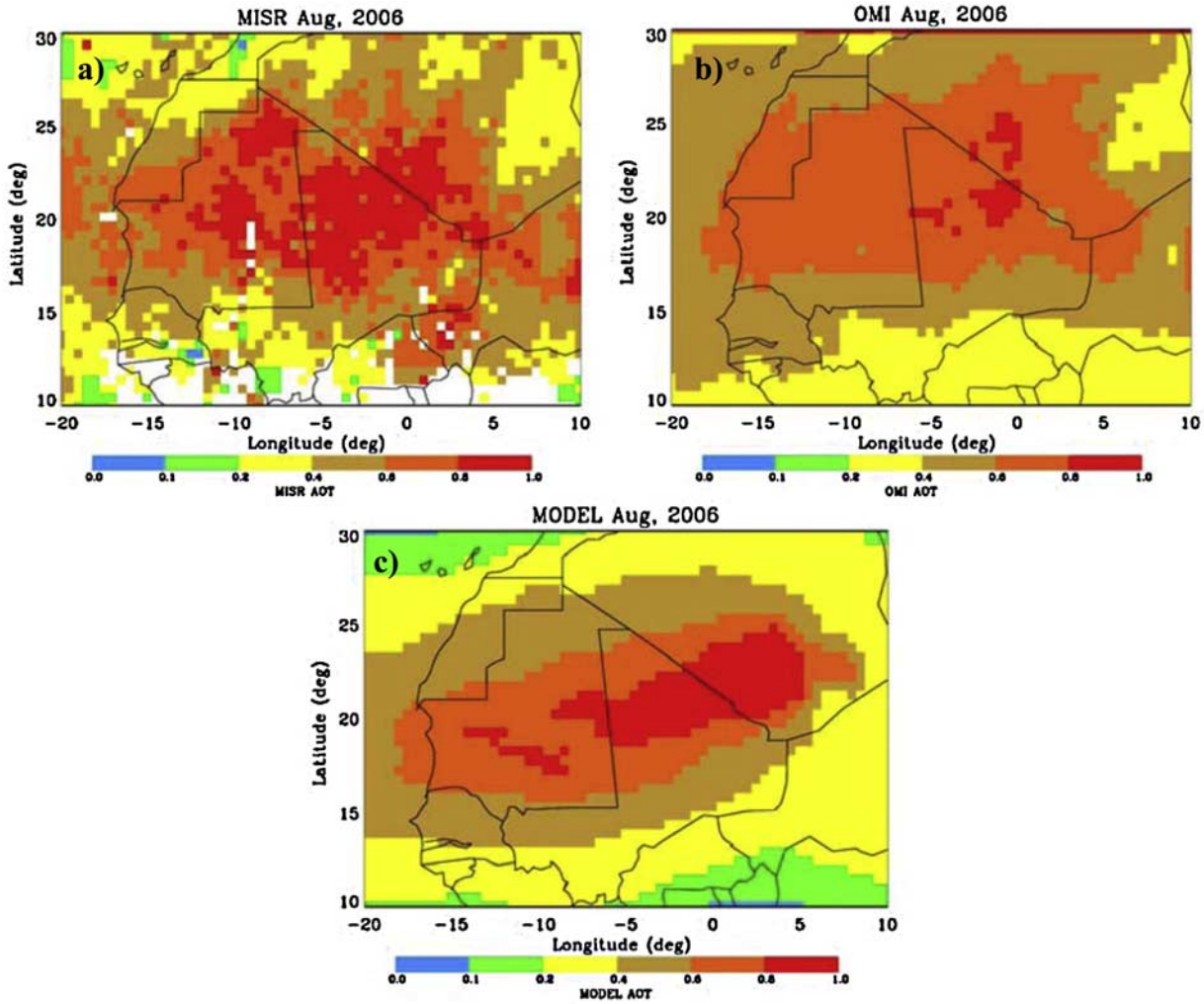

Figure 8. Showing the aerosol optical depth at 550 nm derived from (a) MISR, (b) OMI, (c) and CAMM.

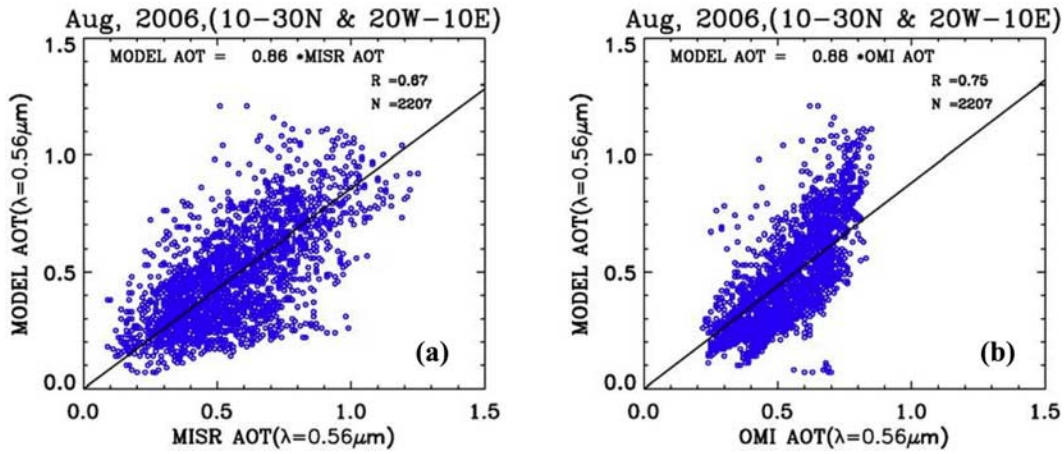

Figure 9. Scatterplots showing (a) MISR AOD versus CAMM AOD and (b) OMI AOD versus CAMM AOD.

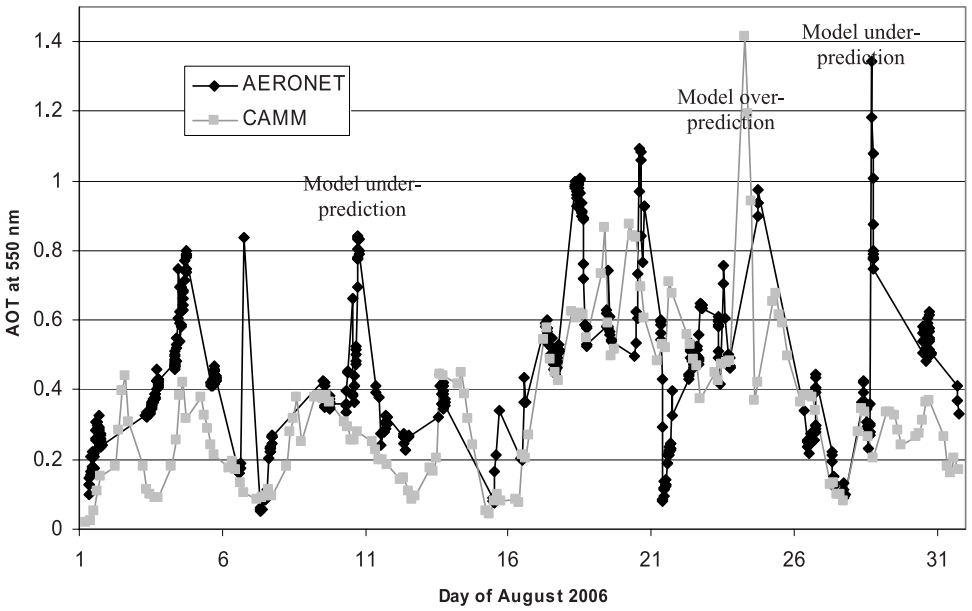

Figure 10. The AOD at 550 nm from the CAMM and AERONET site at M'Bour near Dakar, Senegal for all of August 2006. Only CAMM data from 0600–1800 UT are shown as this roughly corresponds to times when AERONET data can be retrieved (sunlight hours only).

and

$$\mathrm{AOD_{CAMM}} = 1.15\mathrm{AOD_{OMI}} - 0.14$$

if not forced through the origin or

$$\mathrm{AOD_{CAMM}} = 0.86\mathrm{AOD_{MISR}}$$

and

$$\mathrm{AOD_{CAMM}} = 0.88\mathrm{AOD_{OMI}}$$

if forced through the origin (shown in Figure 9). Thus it appears that the AOD from the model is some 12–14% lower than the AOD derived from the satellite instruments. This level of uncertainty appears acceptable, particularly if one considers that the satellite retrievals are not just sensitive to mineral dust, but to all aerosols including sea salt, biogenic, and pollution aerosols. The relationship between $\mathrm{AOD_{MISR}}$ and $\mathrm{AOD_{OMI}}$ can be seen to be close to 1:1 when the regressions are forced through the origin, which shows that the multiyear monthly mean relationship between the two derived by *Christopher et al.* [2008] can be applied to data from 2006.

[34] A comparison of the AOD from the AERONET site of M'Bour near Dakar with that derived from a single-grid box in the model is shown in Figure 10. The mean and standard deviation in the AOD are 0.44 and 0.23 from the AERONET site and 0.34 and 0.23 from the CAMM, and thus the CAMM appears to be able to represent both the mean and the variability reasonably well. Some other events appear well represented on shorter 7-days timescales, such as the generally higher AODs evident in both the model and the observations between 17 and 25 August. However, there are some single day events that are not well represented. For example the CAMM misses the dust events on the 10 and 28 August, and overdoes the magnitude of the dust storm (investigated in the case study) on the 24 August. It should be noted that Figure 10 depicts daily 0600 UT CAMM data, from $T + 0$ to $T + 12$ at 3 hourly intervals, spanning the daylight hours. The AERONET retrievals are available at higher frequency during cloud-free daylight hours, so the data is not exactly synchronous or coherent. Nevertheless, the CAMM appears to capture both the mean and the variability of the AOD reasonably well. Short-range forecast data minimizes any NWP errors and concentrates the comparison upon the models capability to resolve the daily variability of dust. Dust loadings are unconstrained throughout the forecast period, initiated with zero dust in mid-July 2006.

6. Discussion and Conclusions

[35] This study implements a dust scheme developed in a climate model into a higher resolution mesoscale model. A validation strategy including satellite and surface remote sensing measurements and in situ validation using in situ aircraft measurements is developed and implemented. The development of the AOD diagnostic for OMI derived from multiyear correlations of the broad swath TOMS/OMI data against narrow swath MISR instrument [*Christopher et al.*, 2008] proves a useful tool for model validation for individual dust storms. The aircraft measurements show that although the dust size distribution in the model is biased to small sizes, many other features such as the AOD, the vertical profile, and the increased altitude of the surface layer of dust for higher AODs is well represented. The AODs from AERONET and the model show reasonable agreement throughout the entire month of August, although

the model does not represent all the dust events accurately. The dust scheme is known to have a number of weaknesses; the dust availability data set, soil moisture, transport of dust at boundaries and the inability to resolve small-scale dust events Additionally, the domain chosen will have a significant impact upon the dust forecast performance. Encompassing each of the major (upwind) source regions is vital to represent dust variability. The domain chosen here was a balance between including many source areas, the available computer resources to run the operational model and the possible flight areas for the BAe 146 during its flight detachments. A larger domain would be beneficial (1) for including source areas in Eastern Africa and the Middle East and (2) to move the boundaries further away from the domain of interest, mitigating the boundary dust transport limitation. However, the agreement between AODs from the model and the validation measurements for both the individual dust events and the monthly means is very encouraging and shows that the dust model does indeed have predictive skill up to $T + 42$.

[36] There are a number of unresolved issues relating to the dust model which include the bias of the model size distribution to small sizes as evidenced by the wavelength dependence of the aerosol scattering when compared to aircraft observations. This may explain why the dust model appears to transport too much aerosol at high altitudes as the gravitational settling time for small particles is larger than for large particles. Additionally, it is unclear whether the model would perform well if relocated to another area of interest, e.g., the Middle East or whether a further domain-dependent retune might be necessary for accurate representation of the AOD.

[37] **Acknowledgments.** Didier Tanré and Phillippe Gouloub are thanked for maintaining and providing data from the M'Bour AERONET site. The staff of FAAM and Direct Flight are thanked for providing a thoroughly professional service during both DABEX and DODO measurement campaigns.

References

Anderson, T. L., and J. A. Ogren (1998), Determining aerosol radiative properties using the TSI 3563 integrating nephelometer, *Aerosol Sci. Technol.*, *29*, 57–69, doi:10.1080/02786829808965551.

Best, M. J., and P. E. Maisey (2002), A physically based soil moisture nudging scheme, Tech. Note 35, Hadley Centre, Exeter, U. K. (Available at http://www.met-office.gov.uk/research/hadleycentre/pubs/HCTN/HCTN_35.pdf)

Bond, T. C., T. L. Anderson, and D. Campbell (1999), Calibration and intercomparison of filter-based measurements of visible light absorption by aerosols, *Aerosol Sci. Technol.*, *30*, 582–600, doi:10.1080/027868299304435.

Bush, M., S. Bell, N. Christidis, B. MacPherson, R. Renshaw, and C. Wilson (2006), Development of the North Atlantic European Model (NAE) into an operational model, *Forecasting Tech. Rep. 470*, Met Office, Exter, U. K.

Christensen, J. H. (1997), The Danish eulerian hemispheric model—A three-dimensional air pollution model used for the Arctic, *Atmos. Environ.*, *31*, 4169–4191, doi:10.1016/S1352-2310(97)00264-1.

Christopher, S. A., P. Gupta, J. M. Haywood, and G. Greed (2008), Aerosol optical thicknesses over North Africa: 1. Development of a product for model validation using Ozone Monitoring Instrument, Multiangle Imaging Spectroradiometer, and Aerosol Robotic Network, *J. Geophys. Res.*, *113*, D00C04, doi:10.1029/2007JD009446.

Cullen, M. J. P. (1993), The unified forecast/climate model, *Meteorol. Mag.*, *122*(1559), 81–94.

Davies, T., M. J. P. Cullen, A. J. Malcolm, M. H. Mawson, A. Staniforth, A. A. White, and N. Wood (2005), A new dynamical core for the Met Office global and regional modeling of the atmosphere, *Q. J. R. Meteorol. Soc.*, *131*, 1759–1782, doi:10.1256/qj.04.101.

Edwards, J. M., and A. Slingo (1996), Studies with a flexible new radiation code, part 1, Choosing a configuration for a large-scale model, *Q. J. R. Meteorol. Soc.*, *122*, 689–719, doi:10.1002/qj.49712253107.

Essery, R. L. H., M. J. Best, R. A. Betts, P. M. Cox, and C. M. Taylor (2003), Explicit representation of subgrid heterogeneity in a GCM land-surface scheme, *J. Hydrometeorol.*, *4*, 530–543, doi:10.1175/1525-7541(2003)004<0530:EROSHI>2.0.CO;2.

Ginoux, P., and O. Torres (2003), Empirical TOMS index for dust aerosol: Applications to model validation and source characterization, *J. Geophys. Res.*, *108*(D17), 4534, doi:10.1029/2003JD003470.

Greed, G. (2005), Upgrades to the crisis area mesoscale model service, *Forecasting Res. Tech. Rep. 464*, Met Office, Exter, U. K.

Haywood, J. M., and O. Boucher (2000), Estimates of the direct and indirect radiative forcing due to tropospheric aerosols: A review, *Rev. Geophys.*, *38*, 513–543, doi:10.1029/1999RG000078.

Haywood, J. M., P. Francis, S. R. Osborne, M. Glew, N. Loeb, E. Highwood, D. Tanré, G. Myhre, P. Formenti, and E. Hirst (2003), Radiative properties and direct radiative effect of Saharan dust measured by the C-130 aircraft during SHADE: 1. Solar spectrum, *J. Geophys. Res.*, *108*(D18), 8577, doi:10.1029/2002JD002687.

Haywood, J. M., R. P. Allan, I. Culverwell, A. Slingo, S. Milton, J. Edwards, and N. Clerbaux (2005), Can desert dust explain the outgoing longwave radiation anomaly over the Sahara during July 2003?, *J. Geophys. Res.*, *110*, D05105, doi:10.1029/2004JD005232.

Highwood, E. J., J. M. Haywood, M. D. Silverstone, S. M. Newman, and J. P. Taylor (2003), Radiative properties and direct effect of Saharan dust measured by the C-130 aircraft during SHADE: 2. Terrestrial spectrum, *J. Geophys. Res.*, *108*(D18), 8578, doi:10.1029/2002JD002552.

Highwood, E. J., et al. (2007), Aerosol Direct Radiative Impact Experiment (ADRIEX) overview, *Q. J. R. Meteorol. Soc.*, *133*(S1), 3–15.

Holben, B. N., et al. (1998), AERONET—A federated instrument network and data archive for aerosol characterization, *Remote Sens. Environ.*, *66*, 1–16, doi:10.1016/S0034-4257(98)00031-5.

Hotta, S., S. Kubota, S. Katori, and K. Hoikawa (1984), Sand transport by wind on a wet sand surface, paper presented at the 19th Coastal Engineering Conference, Coastal Eng. Res. Counc. of Am. Soc. of Civ. Eng., Houston, Tex.

Hsu, N. C., J. R. Herman, O. Torres, B. N. Holben, D. Tanré, T. F. Eck, A. Smirnov, B. Chatenet, and F. Lavenu (1999), Comparisons of the TOMS aerosol index with Sun photometer aerosol optical thickness: Results and applications, *J. Geophys. Res.*, *104*, 6269–6279, doi:10.1029/1998JD200086.

In, H.-J., and S.-U. Park (2003), A simulation of long-range transport of yellow sand observed in April 1998 in Korea, *Atmos. Environ.*, *37*, 4625–4636, doi:10.1016/j.atmosenv.2003.07.009.

Intergovernmental Panel on Climate Change (2001), *Climate Change 2001: The Scientific Basis, Contribution of Working Group I to the Third Assessment Report of the Intergovernmental Panel on Climate Change*, edited by J. T. Houghton et al., Cambridge Univ. Press, Cambridge, U. K.

Kallos, G., et al. (1997), The regional weather forecasting system SKIRON: An overview, in *Proceedings of Symposium on Regional Weather Prediction on Parallel Computer Environments*, edited by G. Kallos, V. Kotroni, and K. Lagouvardos, Univ. of Athens, Athens.

Kishcha, P., et al. (2007), Forecast errors in dust vertical distributions over Rome (Italy): Multiple particle size representation and cloud contributions, *J. Geophys. Res.*, *112*, D15205, doi:10.1029/2006JD007427.

Liu, M., D. L. Westphal, S. Wang, A. Shimizu, N. Sugimoto, J. Zhou, and Y. Chen (2003), A high-resolution numerical study of the Asian dust storms of April 2001, *J. Geophys. Res.*, *108*(D23), 8653, doi:10.1029/2002JD003178.

Lock, A. P., A. R. Brown, M. R. Bush, G. M. Martin, and R. N. B. Smith (2000), A new boundary layer mixing scheme. Part I: Scheme description and single column model test, *Mon. Weather Rev.*, *128*, 3187–3199, doi:10.1175/1520-0493(2000)128<3187:ANBLMS>2.0.CO;2.

Lorenc, A. C., et al. (2000), The Met. Office global three-dimensional variational data assimilation scheme, *Q. J. R. Meteorol. Soc.*, *126*, 2991–3012, doi:10.1002/qj.49712657002.

Loveland, T. R., and A. S. Belward (1998), The International Geosphere Biosphere Programme Data and Information System Global Land Cover Data Set (DISCover), *Acta Astronaut.*, *41*(4–10), 681–689.

Marticorena, B., and G. Bergametti (1997), Modeling the atmospheric dust cycle: 2. Simulation of Saharan dust sources, *J. Geophys. Res.*, *102*, 4387–4404, doi:10.1029/96JD02964.

Martin, G. M., M. R. Bush, A. R. Brown, A. P. Local, and R. N. B. Smith (2000), A new boundary layer mixing scheme. Part II: Tests in climate and mesoscale models, *Mon. Weather Rev.*, *128*, 3200–3217, doi:10.1175/1520-0493(2000)128<3200:ANBLMS>2.0.CO;2.

Martonchik, J. V., D. J. Diner, R. Kahn, B. Gaitley, and B. N. Holben (2004), Comparison of MISR and AERONET aerosol optical depths over desert sites, *Geophys. Res. Lett.*, *31*, L16102, doi:10.1029/2004GL019807.

Menut, L., G. Forêt, and G. Bergametti (2007), Sensitivity of mineral dust concentrations to the model size distribution accuracy, *J. Geophys. Res.*, *112*, D10210, doi:10.1029/2006JD007766.

Milton, S. F., G. Greed, M. Brooks, J. M. Haywood, B. Johnson, R. P. Allan, and A. Slingo (2008), Modeled and observed atmospheric radiation balance during the West African dry season: The role of mineral dust, biomass burning aerosol, and surface albedo, *J. Geophys. Res.*, *113*, D00C02, doi:10.1029/2007JD009741.

Nickovic, S., A. Papadopoulos, O. Kakaliagou, and G. Kallos (2001), Model for prediciton of desert dust cycle in the atmosphere, *J. Geophys. Res.*, *106*, 18,113–18,129, doi:10.1029/2000JD900794.

Pérez, C., S. Nickovic, G. Pejanovic, J. M. Baldasano, and E. Özsoy (2006), Interactive dust-radiation modeling: A step to improve weather forecasts, *J. Geophys. Res.*, *111*, D16206, doi:10.1029/2005JD006717.

Rawlins, R., S. Ballard, K. Bovis, A. Clayton, D. Li, G. Inverarity, A. Lorenc, and T. Payne (2007), The Met Office global four-dimensional variational data assimilation scheme, *Q. J. R. Meteorol. Soc.*, *133*, 347–362, doi:10.1002/qj.32.

Slingo, A., et al. (2006), Observations of the impact of a major Saharan dust storm on the atmospheric radiation balance, *Geophys. Res. Lett.*, *33*(24), L24817, doi:10.1029/2006GL027869.

Sterk, G. (2003), Causes, consequences and control of wind erosion in Sahelian Africa: A review, *Land Degrad. Dev.*, *14*, 95–108, doi:10.1002/ldr.526.

Tanaka, T. Y., and M. Chiba (2005), Global simulation of dust aerosol with a chemical transport model, MASINGAR, *J. Meteorol. Soc. Jpn.*, *83A*, 255–278, doi:10.2151/jmsj.83A.255.

Uno, I., et al. (2006), Dust model intercomparison (DMIP) study over Asia: Overview, *J. Geophys. Res.*, *111*, D12213, doi:10.1029/2005JD006575.

Wilson, M. F., and A. Henderson-Sellers (1985), A global archive of land cover and soils data for use in general circulation climate models, *Int. J. Climatol.*, *5*, 119–143, doi:10.1002/joc.3370050202.

Woodward, S. (2001), Modeling the atmospheric life cycle and radiative impact of mineral dust in the Hadley Centre climate model, *J. Geophys. Res.*, *106*(D16), 18,155–18,166, doi:10.1029/2000JD900795.

S. Christopher and P. Gupta, Department of Atmospheric Sciences, University of Alabama in Huntsville, 320 Sparkman Drive, Huntsville, AL 35806, USA.

G. Greed, J. Haywood, A. Keil, and S. Milton, Met Office, FitzRoy Road, Exeter EX1 3PB, UK. (jim.haywood@metoffice.com)

E. Highwood, Department of Meteorology, University of Reading, Whiteknights, P.O. Box 217, Reading RG6 6AH, UK.